

# Nanocircuit transmitting microwave and terahertz harmonics generated by a mode-locked laser

Mark J. Hagmann, Department of Electrical and Computer Engineering,  
University of Utah, Salt Lake City, Utah 84112, and Isaac Martin

## Abstract

Earlier we focused a mode-locked laser on the tip-sample tunneling junction of a scanning tunneling microscope. This superimposed currents at hundreds of harmonics of the laser pulse-repetition rate on the DC tunneling current. The power at each harmonic is inversely proportional to its frequency. However, analysis suggests that within the tunneling junction the harmonics only decay above 45 THz as the exponent of minus the square of the product of the harmonic number and the laser duty cycle. Now this effect is applied in a nanocircuit with an optical antenna to receive the laser radiation, metal-insulator-metal tunneling diodes to generate the harmonics, and filters to select the microwave or terahertz harmonics that are transmitted by a second antenna.

## 1. Background and introduction

Guided by simulations, we focused a mode-locked Ti:Sapphire laser on the tunneling junction of a scanning tunneling microscope (STM) to generate a unique microwave frequency comb (MFC) [1]. There are hundreds of harmonics at integer multiples of the 74.25 MHz laser pulse-repetition frequency. This may be understood because the tip-sample distance is much shorter than the wavelengths of the laser so at nanoscale the effectively the laser superimposes a time-dependent voltage on the DC bias of the STM.

The 200<sup>th</sup> harmonic, at 14.85 GHz, has a power of only 2.8 atto-watts with an applied DC tunneling current of 10  $\mu$ A. However, its signal-to-noise ratio is 25 dB because the FWHM (full-width at half-maximum) linewidth of 1.2 Hz for each harmonic reduces the received background noise. However, this measured linewidth is an upper bound as a convolution of the actual linewidth with the response of the spectrum analyzer. Thus, the quality factor (Q) exceeds  $10^{10}$  as the state-of-the-art for low-noise in microwave measurements [2].

Figure 1 is a block diagram for the system we used to measure the microwave harmonics with a miniature 50- $\Omega$  coaxial cable connecting the STM tip to a digital spectrum analyzer.

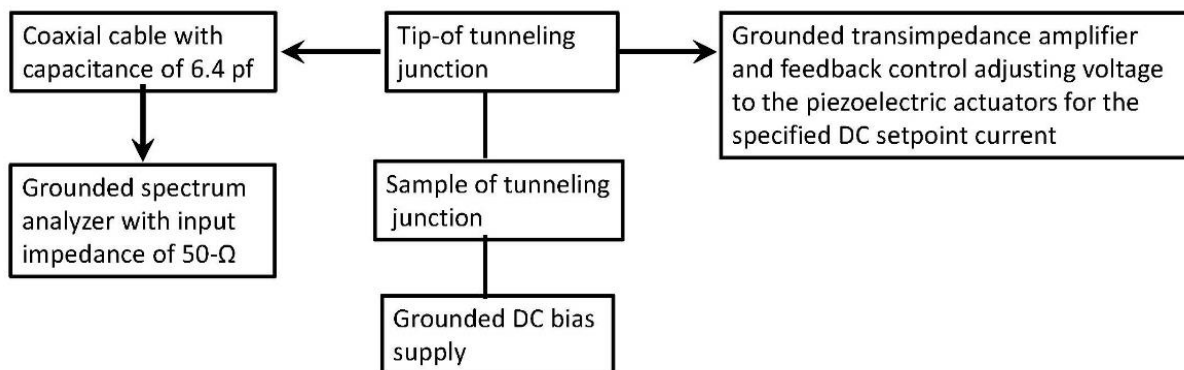


Fig. 1. Block diagram of the system used to measure the microwave harmonics with an STM.

The resistance of the tunneling junction is much greater than the characteristic impedance of the cable. Thus, the cable acts as a capacitance of 6.4 pF across the 50- $\Omega$  input impedance of the spectrum analyzer. The current at each harmonic is divided between the spectrum analyzer and the capacitive shunt presented by the cable. This forms a low-pass filter, with a 3dB point of 500 MHz. Thus, the total power measured by the spectrum analyzer for the first N harmonics is given by Eq. (1) where R is the input impedance of the spectrum analyzer, C is the shunting capacitance of the miniature coaxial cable, and  $\omega_I$  is the angular frequency of the I-th harmonic. Later in this paper we will consider the fundamental limit to this type of measurement that becomes dominant at a frequency of 45 THz [3].

Using the parameters for Eq. (1) it is seen that the second term in the denominator is dominant so Eq. (2) may be used with the STM measurements. Thus far we have only measured the first 200 harmonics with the STM, and the roll-off in the power at these harmonics is consistent with all of the  $P_I$  being equal so we set  $P_I$  to  $P_1$ , the power at the first harmonic. We define  $\omega_I$  as  $I\omega_0$  where  $\omega_0$  is the angular frequency corresponding to the pulse-repetition rate of the laser to obtain Eq. (3). In the limit as N becomes large Eq. (3) approaches the limit that is given in Eq. (4) to estimate of the total power for the harmonics in the STM, where now  $f_0$  is the pulse-repetition rate of the mode-locked laser.

$$P_{tot} = \sum_{I=1}^N \frac{P_I}{1 + \omega_I^2 R^2 C^2} \quad (1)$$

$$P_{tot} = \frac{1}{R^2 C^2} \sum_{I=1}^N \frac{P_I}{\omega_I^2} \quad (2)$$

$$P_{tot} = \frac{P_1}{\omega_0^2 R^2 C^2} \sum_{I=1}^N \frac{1}{I^2} \quad (3)$$

$$P_{tot} = \frac{P_1}{24 f_0^2 R^2 C^2} \quad (4)$$

A power of -86 dBm (2.5 pW) was measured in the STM at the first harmonic where  $f_0$  is 74.25 MHz when using an R of 50  $\Omega$  and C equal to 6.4 pF with a DC tunneling current of 50  $\mu$ A [4]. Thus, Eq. (4) shows that the total power for all of the harmonics was 73.8 times greater than that at the first harmonic, or  $73.8 \times 2.5 \times 10^{-12}$  W which is 0.18 nW.

We would suggest that these harmonics are not merely a perturbation of the DC tunneling current due to the nonlinear dependence of the current on the applied bias voltage in an STM. This possibility becomes clear in our analysis and simulations of Scanning Frequency Comb Microscopy (SFCM) where the harmonics would be used for feedback control of the tip-sample distance in an STM without an applied DC bias.

We acknowledge that SFCM would require resistive samples such as semiconductors, and it has been analyzed, and simulated, but not yet tested [5],[6],[7]. In SFCM, first tunneling would be established using feedback control of the tip-sample separation to provide a specified setpoint value for the DC tunneling current. Then the DC bias would be turned off and feedback control of the tip-sample distance would be based on the measured power of the microwave frequency comb. Feedback control of the tip-sample distance would be accomplished by adjusting the tip-sample distance to maximize the power measured at the harmonics. This may be understood because, at distance for maximum power, (1) reducing the tip-sample distance from this point increases the spreading resistance by causing the harmonics to pass through a cross-sectional smaller area in the

sample, while (2) increasing the tip-sample distance increases the tunneling resistance to reduce the current in the harmonics.

Now we consider the possibility of fabricating nanocircuits in which higher harmonics may be generated without the need for feedback control while mitigating the roll-off in the output power at higher frequencies that occurs with an STM. The nanocircuits will use symmetric MIM diodes with a size that is considerably less than that of the tip and the sample electrode in an STM which increases the ratio of the surface area to the volume to provide greater heat transfer facilitating the use of much greater current densities. Optical antennas will receive the radiation from a mode-locked laser and an antenna will transmit selected harmonics at microwave and/or terahertz frequencies (patent-pending).

## 2. Description of the new nanocircuit

Figure 2 is a sketch of the design for the new nanocircuit. Here “MIM” denotes each of the two symmetrical metal-insulator-metal tunneling diodes that replace the STM tunneling junction. No semiconductors are required. Each MIM diode will be made by making a small gap in the metal lead, coating this gap with a refractory metal, and using ion beam lithography to form a sub-nanometer gap in the refractory metal. The components are attached to a substrate having a low dielectric constant to limit coupling to the transmitting antenna and other components. This sketch is not made to scale.

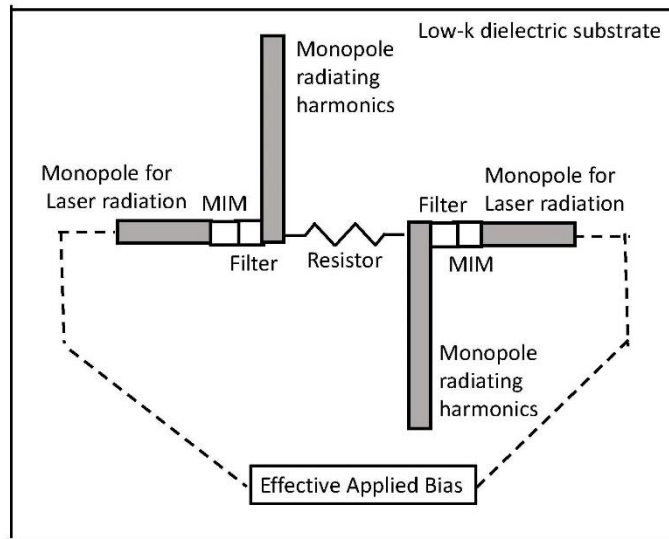


Fig. 2. Sketch of the nanocircuit generating microwave and terahertz harmonics.

Instead of focusing a laser on the tunneling junction of an STM, the laser will excite the monopole optical nanoantennas shown at the left and right ends of the sketch. This will cause a voltage having the full spectrum of the laser across each MIM diode that is labeled as the “effective applied bias” to relate this to our STM measurements. The mode-locked laser will have a precision power splitter with a phase shifter to be focused simultaneously on the two optical nanoantennas.

The two filters prevent the spectrum of the laser from reaching the circuit between them. Thus, only the current at the harmonics generated in the two MIM diodes passes through the resistor at the center of the sketch. This resistor is across the feed-point for the dipole that is formed by the two vertical monopole antennas. Thus, the voltage across this resistor feeds the vertical

dipole to radiate at microwave or terahertz harmonics that are selected by the two filters. Nanoscale resistive L-type networks may be included to provide broadband impedance matching.

### 3. Method for generating the tunneling current in the MIM diodes

Focusing a laser normal to the outer electrode of each MIM diode would not cause optimum electron transport within the MIM diode by quantum tunneling because the incident electric field from the laser would be tangential to the electrode. One method to solve this problem is shown in Fig. 3 where the laser radiation passes horizontally across the surface of the outer electrode in each MIM diode. The electric field from the laser is normal to the surface of this electrode to cause the electrons to be displaced vertically within the metal as shown to create electrical charges with opposite signs on the upper and lower surfaces. Thus, there is a vertical electric field between the two electrodes of each MIM diode to cause electrons to tunnel between them as shown in Fig. 3. In this case the optical antennas receiving the laser radiation could be vertical metallic nanotips attached to the electrode. It is also possible for the surface of the electrode to act as an antenna. The width of each electrode for the MIM diodes is much less than the wavelengths of the laser so this is a quasistatic process. This sketch is not made to scale.

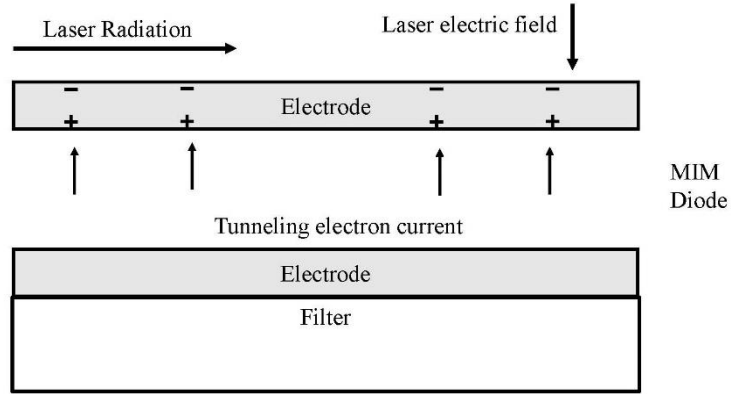


Fig. 3. Sketch of the MIM diode with the laser causing an electric field normal to the outer electrode.

### 4. General expression for the current in each MIM tunneling diode

In a previous analysis we showed that, if the harmonics could be measured within a tunneling junction, the power at the  $k$ -th harmonic would be given by Eq. (5) where  $P_1$  is the value at the first harmonic [3]. Thus, Eq. (6) gives the current at the  $k$ -th harmonic where  $I_1$  is the magnitude of the current at the first harmonic. Here  $T$  is the period for each cycle of the mode-locked laser and  $\tau$  is the duration of each laser pulse. The duty cycle,  $\tau/T$ , is extremely small. Thus, in STM measurements [1], where a power of -120 dBm was measured at the first harmonic with a spectrum analyzer having an input impedance of  $50 \Omega$ ,  $I_1$  was approximately 6 nA.

$$P_k = P_1 e^{-\pi^2(k-1)^2 \left(\frac{\tau}{T}\right)^2} \quad (5)$$

$$I_k = I_1 \sin(k\omega_0 t) e^{-\frac{\pi^2 \tau^2}{2T^2} (k-1)^2} \quad (6)$$

Equation (6) is simplified to give Eq. (7) where  $A$  is an extremely small parameter defined in Eq. (8) and  $k$  is the harmonic number. We refer to the phenomena occurring where  $Ak^2$  is comparable to unity as the “cutoff” because the exponential decay of the current that is caused by the physics is first prominent in the harmonics above that point.

$$I_k = I_1 \sin(k\omega_0 t) e^{-Ak^2} \quad (7)$$

$$A \equiv \frac{\pi^2}{2} \left( \frac{\tau}{T} \right)^2 \quad (8)$$

The analysis that resulted in Eq. (5) did not allow for the effects of the capacitance  $C$  shunting the tunneling junction or the load resistance  $R$ , but these effects were included in Eqs. (1), (2), (3), and (4) for the analysis with an STM. However, the capacitance of each MIM diode in the nanocircuit may be much less than 1 femto-Farad so we make the approximation of neglecting these effects. Thus, with the nanocircuits, we add the powers at all of the harmonics to obtain the total power to the load.

## 5. Components of the electrical current within the nanocircuit

Figure 4 is a diagram showing the components of the current within the nanocircuit. The filtered current from the MIM diode at the left splits into two parts, one going through the resistor and the other to the upper monopole. The current going through the resistor splits into two parts, one going to the second filtered MIM diode and the other going through the lower monopole. Determining these currents would require knowing the radiation resistance, loss-resistance, and reactance of each vertical monopole, the value of the resistor, and the spectrum of the filtered current from the two MIM diodes.

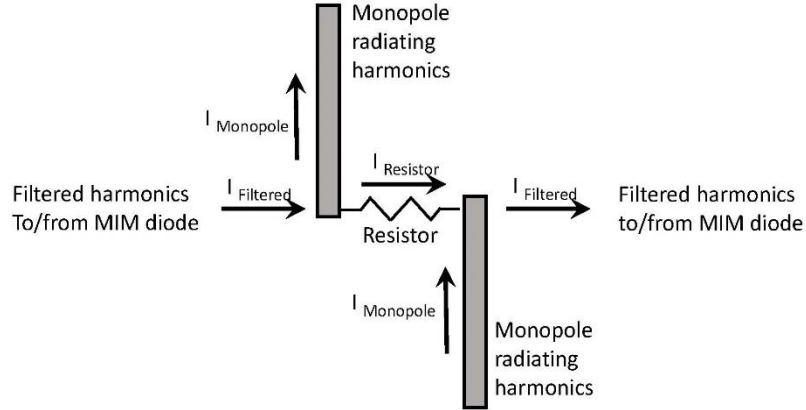


Fig. 4. Components of the current within the nanocircuit.

## 6. Possibility of using several microwave harmonics or many at terahertz frequencies

In applying this technology, the part of the full spectrum of harmonics that is transmitted is determined by the two filters as well as the properties of the antenna transmitting the harmonics. At microwave frequencies it is possible to transmit one or several individual harmonics. However, at terahertz frequencies the spacing between adjacent harmonics is much smaller than their individual frequencies so present filter technology cannot be used to separate the individual harmonics. Sets of adjacent harmonics are of special interest because the larger number of harmonics used at terahertz frequencies (e.g., 1000) can transmit much higher power.

Here we consider the effect of transmitting a set of adjacent harmonics where the fundamental frequency  $\omega_0$ , which is the angular form of the pulse repetition rate for the laser, is defined in Eq. (9). Thus, at time  $t$ , the total current from these harmonics is given by Eq. (10).

$$\omega_k \equiv k\omega_0, \text{ where the integer } k_1 \leq k \leq k_2 \quad (9)$$

$$I(t) = I_1 \sum_{k=k_1}^{k_2} \sin(k\omega_0 t) e^{-Ak^2} \quad (10)$$

Next, we will solve Eq. (10) to obtain closed-form algebraic expressions for the total current in different sets of adjacent harmonics that are well below the cutoff (Section 7), and near to the cutoff (Section 8), as well as in general case (Section 9).

### 7. Derivation for the current in a set of adjacent harmonics well below the cutoff

As already noted, at the higher harmonics, the exponential in Eq. (10) causes a cutoff where the current decays to zero. However, in this section we make the approximation of setting this exponential to unity to study a set of harmonics that are well below the cutoff. We derived the identity in Eq. (11) using Wolfram Alpha, verified it, and then used it with Eq. (10) to obtain Eq. (12) for the total current as a function of time with all of the harmonics in the interval  $k_1 \leq k \leq k_2$ . The numerical testing included several examples where the terms for each value of  $k$  were calculated at different time-steps using Eq. (10) and then summed. These sums at each time-step were then compared with the values found using the closed-form solution in Eq. (12).

$$\sum_{k=k_1}^{k_2} \sin(kx) \equiv \frac{1}{2} \left[ \begin{array}{l} \sin(k_1 x) + \cot\left(\frac{x}{2}\right) \cos(k_1 x) \\ + \sin(k_2 x) - \cot\left(\frac{x}{2}\right) \cos(k_2 x) \end{array} \right] \quad (11)$$

$$I(t) = \frac{I_1}{2} \left[ \begin{array}{l} \sin(k_1 \omega_0 t) + \cot\left(\frac{\omega_0 t}{2}\right) \cos(k_1 \omega_0 t) \\ + \sin(k_2 \omega_0 t) - \cot\left(\frac{\omega_0 t}{2}\right) \cos(k_2 \omega_0 t) \end{array} \right] \quad (12)$$

### 8. Derivation of the current in a set of adjacent harmonics near the cutoff

Let  $\|I_k\|$  be defined as the peak value for the current at the  $k$ th harmonic. Thus, because the spacing between adjacent harmonics is small near the cutoff, the value for the peak of the  $k+1$  harmonic is related to that for the  $k$ -th harmonic by the approximation in Eq. (13):

$$\frac{\|I_{k+1}\|}{\|I_k\|} = \frac{e^{-A(k+1)^2}}{e^{-Ak^2}} \approx e^{-A(2k+1)} \quad (13)$$

The Ti:Sapphire laser used in our measurements at Los Alamos has a pulse duration  $\tau$  of 6 fs, and a pulse repetition rate of 74.25 MHz so the time between consecutive pulses  $T$  is 13.5 ns. Thus, from Eq. 8, the dimensionless parameter  $A$  is  $9.7 \times 10^{-13}$ . In order to determine the value of  $k$  at which the peak power has decayed to one-half of that at the fundamental we label this value as  $k_{3dB}$  to obtain Eq. (14), and write Eq. (15) for the current at the fundamental where  $k$  is 1.

$$\|I_{k_{3dB}}\| = I_1 e^{-Ak_{3dB}^2} \quad (14)$$

$$\|I_1\| = I_1 e^{-A} \quad (15)$$

Equation (16) is obtained by combining Eqs. (14) and (15), so the ratio of these two values of power is given by Eq. (17). To determine the value of  $k$  at the 3-dB point this ratio is set to one-half to obtain Eq. (18) which is rearranged to give Eq. (19), Eq. (20), and finally Eq. (21) as the index  $k$  at the 3-dB point.

$$\frac{\|I_{k_{3dB}}\|}{\|I_1\|} = e^{-Ak_{3dB}^2} \quad (16)$$

$$\frac{P_{k_{3dB}}}{P_1} = e^{2A-2Ak_{3dB}^2} \quad (17)$$

$$2e^{2A-2Ak_{3dB}^2} = 1 \quad (18)$$

$$\ln(2) = 2Ak_{3dB}^2 - 2A \quad (19)$$

$$\frac{\ln(2)}{2A} + 1 = k_{3dB}^2 \quad (20)$$

$$k_{3dB} = \sqrt{1 + \frac{\ln(2)}{2A}} \quad (21)$$

Earlier in this section we noted that in our measurements of the microwave frequency comb with an STM the parameter  $A$  was approximately  $9.7 \times 10^{-13}$ . Thus, Eq. (21) shows that under these conditions  $k_{3dB}$  would be  $6.0 \times 10^5$  which shows that the cutoff would be near 45 THz [3].

Next, we consider how to determine the total current as a function of time for a small band of harmonics with  $k_1 \leq k \leq k_2$  where  $k_1$  and  $k_2$  are large integers. When the range  $k_2$  minus  $k_1$ , is much smaller than either  $k_1$  or  $k_2$  there will be little variation in the value of the exponential in Eq. (10). Thus, we approximate Eq. (10) with Eq. (22) where  $\bar{k}$  is defined as the mean value for  $k_1$  and  $k_2$ . Then the summation in Eq. (11) is used with Eq. (22) to obtain Eq. (23) as an approximation for the total current in the harmonics from  $k_1$  to  $k_2$ . However, we anticipate that actual measurements of the spectrum of the harmonics that are close to the cutoff may be sensitive to the stability of the mode-locked laser.

$$I(t) = I_1 e^{-A\bar{k}^2} \sum_{k=k_1}^{k=k_2} \sin(k\omega_0 t) \quad (22)$$

$$I(t) = \frac{I_1}{2} e^{-A\bar{k}^2} \left[ \begin{aligned} &\sin(k_1\omega_0 t) + \cot\left(\frac{\omega_0 t}{2}\right) \cos(k_1\omega_0 t) \\ &+ \sin(k_2\omega_0 t) - \cot\left(\frac{\omega_0 t}{2}\right) \cos(k_2\omega_0 t) \end{aligned} \right] \quad (23)$$

## 9. Derivation of the current in any set of adjacent harmonics

The Taylor series expansion for the exponential in Eq. (10) is given by Eq. (24)

$$e^{-Ak^2} = \sum_{n=0}^{\infty} \frac{(-Ak^2)^n}{n!} \quad (24)$$

Combining Eqs. (10) and (24) gives Eq. (25) for the total current where  $x$  is  $\omega_0 t$ .

$$I(t) = I_1 \sum_{k=k_1}^{k=k_2} \left[ \sin(kx) \sum_{n=0}^{\infty} \frac{(-Ak^2)^n}{n!} \right] \quad (25)$$

Writing the first few terms of the summation in Eq. (25) gives Eq. (26) for the total current.

$$I(t) = I_1 \sum_{k=k_1}^{k=k_2} \left[ \sin(kx) \left\{ 1 - \frac{Ak^2}{1!} + \frac{A^2 k^4}{2!} - \frac{A^3 k^6}{3!} + \frac{A^4 k^8}{4!} - \frac{A^5 k^{10}}{5!} + \dots \right\} \right] \quad (26)$$

Next, the first six terms of the inner summation in Eq. (26) are separated to give 6 parts where the first one, denoted by  $T_1$ , is Eq. (27) which was derived earlier as Eq. (11). The definitions of the other 5 other terms in Eq. (26), and closed-form expressions from Wolfram Alpha which we have confirmed, are given in Eqs. (28) through (32).

$$T_1 \equiv \sum_{k=k_1}^{k_2} \sin(kx) = \frac{1}{2} \left[ \sin(k_1 x) + \cot\left(\frac{x}{2}\right) \cos(k_1 x) + \sin(k_2 x) - \cot\left(\frac{x}{2}\right) \cos(k_2 x) \right] \quad (27)$$

$$T_2 \equiv -\frac{A}{1!} \sum_{k=k_1}^{k_2} k^2 \sin(kx) = -\frac{A}{1} x^2 \csc\left(\frac{x}{2}\right) \sin\left[\frac{1}{2}(1-k_1+k_2)x\right] \sin\left[\frac{1}{2}(n_1+n_2)x\right] \quad (28)$$

$$T_3 \equiv \frac{A^2}{2!} \sum_{k=k_1}^{k_2} k^4 \sin(kx) = \frac{A^2}{2!} x^4 \csc\left(\frac{x}{2}\right) \sin\left[\frac{1}{2}(1-k_1+k_2)x\right] \sin\left[\frac{1}{2}(k_1+k_2)x\right] \quad (29)$$

$$T_4 \equiv -\frac{A^3}{3!} \sum_{k=k_1}^{k_2} k^6 \sin(kx) = -\frac{A^3}{3!} x^6 \csc\left(\frac{x}{2}\right) \sin\left[\frac{1}{2}(1-k_1+k_2)x\right] \sin\left[\frac{1}{2}(k_1+k_2)x\right] \quad (30)$$

$$T_5 \equiv \frac{A^4}{4!} \sum_{k=k_1}^{k_2} k^8 \sin(kx) = \frac{A^4}{4!} x^8 \csc\left(\frac{x}{2}\right) \sin\left[\frac{1}{2}(1-k_1+k_2)x\right] \sin\left[\frac{1}{2}(k_1+k_2)x\right] \quad (31)$$

$$T_6 \equiv -\frac{A^5}{5!} \sum_{k=k_1}^{k_2} k^{10} \sin(kx) = -\frac{A^5}{5!} x^{10} \csc\left(\frac{x}{2}\right) \sin\left[\frac{1}{2}(1-k_1+k_2)x\right] \sin\left[\frac{1}{2}(k_1+k_2)x\right] \quad (32)$$

Setting  $x$  to  $\omega_0 t$  and simplifying Eqs. (27) to (32) gives Eqs. (33) through (38).

$$T_1 = \frac{1}{2} \left[ \sin(k_1 \omega_0 t) + \cot\left(\frac{\omega_0 t}{2}\right) \cos(k_1 \omega_0 t) + \sin(k_2 \omega_0 t) - \cot\left(\frac{\omega_0 t}{2}\right) \cos(k_2 \omega_0 t) \right] \quad (33)$$

$$T_2 = -\frac{A}{1} (\omega_0 t)^2 \csc\left(\frac{\omega_0 t}{2}\right) \sin\left[\frac{1}{2}(1-k_1+k_2)\omega_0 t\right] \sin\left[\frac{1}{2}(k_1+k_2)\omega_0 t\right] \quad (34)$$

$$T_3 = \frac{A^2}{2!} (\omega_0 t)^4 \csc\left(\frac{\omega_0 t}{2}\right) \sin\left[\frac{1}{2}(1-k_1+k_2)\omega_0 t\right] \sin\left[\frac{1}{2}(k_1+k_2)\omega_0 t\right] \quad (35)$$

$$T_4 = -\frac{A^3}{3!} (\omega_0 t)^6 \csc\left(\frac{\omega_0 t}{2}\right) \sin\left[\frac{1}{2}(1-k_1+k_2)\omega_0 t\right] \sin\left[\frac{1}{2}(k_1+k_2)\omega_0 t\right] \quad (36)$$

$$T_5 = \frac{A^4}{4!} (\omega_0 t)^8 \csc\left(\frac{\omega_0 t}{2}\right) \sin\left[\frac{1}{2}(1-k_1+k_2)\omega_0 t\right] \sin\left[\frac{1}{2}(k_1+k_2)\omega_0 t\right] \quad (37)$$

$$T_6 = -\frac{A^5}{5!} (\omega_0 t)^{10} \csc\left(\frac{\omega_0 t}{2}\right) \sin\left[\frac{1}{2}(1-k_1+k_2)\omega_0 t\right] \sin\left[\frac{1}{2}(k_1+k_2)\omega_0 t\right] \quad (38)$$

Thus, the total current as a function of time is obtained by multiplying  $I_1$  by the sum of the RHS in Eqs. (33) through (38) to obtain Eq. (39), recognizing that Eq. (39) must be continued as shown by the ellipsis, where this is factored to obtain Eq. (40).

$$\begin{aligned}
I(t) = & \frac{I_1}{2} \left[ \sin(k_1 \omega_0 t) + \cot\left(\frac{\omega_0 t}{2}\right) \cos(k_1 \omega_0 t) + \sin(k_2 \omega_0 t) - \cot\left(\frac{\omega_0 t}{2}\right) \cos(k_2 \omega_0 t) \right] \\
& - \frac{A I_1}{1!} (\omega_0 t)^2 \csc\left(\frac{\omega_0 t}{2}\right) \sin\left[\frac{1}{2}(1-k_1+k_2)\omega_0 t\right] \sin\left[\frac{1}{2}(k_1+k_2)\omega_0 t\right] \\
& + \frac{A^2 I_1}{2!} (\omega_0 t)^4 \csc\left(\frac{\omega_0 t}{2}\right) \sin\left[\frac{1}{2}(1-k_1+k_2)\omega_0 t\right] \sin\left[\frac{1}{2}(k_1+k_2)\omega_0 t\right] \\
& - \frac{A^3 I_1}{3!} (\omega_0 t)^6 \csc\left(\frac{\omega_0 t}{2}\right) \sin\left[\frac{1}{2}(1-k_1+k_2)\omega_0 t\right] \sin\left[\frac{1}{2}(k_1+k_2)\omega_0 t\right] \\
& + \frac{A^4 I_1}{4!} (\omega_0 t)^8 \csc\left(\frac{\omega_0 t}{2}\right) \sin\left[\frac{1}{2}(1-k_1+k_2)\omega_0 t\right] \sin\left[\frac{1}{2}(k_1+k_2)\omega_0 t\right] \\
& - \frac{A^5 I_1}{5!} (\omega_0 t)^{10} \csc\left(\frac{\omega_0 t}{2}\right) \sin\left[\frac{1}{2}(1-k_1+k_2)\omega_0 t\right] \sin\left[\frac{1}{2}(k_1+k_2)\omega_0 t\right] + \dots \quad (39)
\end{aligned}$$

$$\begin{aligned}
I(t) = & \frac{I_1}{2} \left[ \sin(k_1 \omega_0 t) + \cot\left(\frac{\omega_0 t}{2}\right) \cos(k_1 \omega_0 t) + \sin(k_2 \omega_0 t) - \cot\left(\frac{\omega_0 t}{2}\right) \cos(k_2 \omega_0 t) \right] \\
& - I_1 \left[ \frac{A}{1!} (\omega_0 t)^2 - \frac{A^2}{2!} (\omega_0 t)^4 + \frac{A^3}{3!} (\omega_0 t)^6 - \frac{A^4}{4!} (\omega_0 t)^8 + \frac{A^5}{5!} (\omega_0 t)^{10} - \dots \right] \\
& \csc\left(\frac{\omega_0 t}{2}\right) \sin\left[\frac{1}{2}(1-k_1+k_2)\omega_0 t\right] \sin\left[\frac{1}{2}(k_1+k_2)\omega_0 t\right] \quad (40)
\end{aligned}$$

We use the Taylor series in Eq. (41), rearranged as Eq. (42), with the argument  $x$  changed to obtain Eq. (43). Then this result is used to change the second line of Eq. (40) in order to obtain Eq. (44).

$$e^{-x} = 1 - \frac{x}{1!} + \frac{x^2}{2!} - \frac{x^3}{3!} + \frac{x^4}{4!} - \frac{x^5}{5!} + \dots \quad (41)$$

$$1 - e^{-x} = \frac{x}{1!} - \frac{x^2}{2!} + \frac{x^3}{3!} - \frac{x^4}{4!} + \frac{x^5}{5!} - \dots \quad (42)$$

$$1 - e^{-A(\omega_0 t)^2} \equiv \frac{A(\omega_0 t)^2}{1!} - \frac{A^2(\omega_0 t)^4}{2!} + \frac{A^3(\omega_0 t)^6}{3!} - \frac{A^4(\omega_0 t)^8}{4!} + \frac{A^5(\omega_0 t)^{10}}{5!} - \dots \quad (43)$$

$$\begin{aligned}
I(t) = & \frac{I_1}{2} \left[ \sin(k_1 \omega_0 t) + \cot\left(\frac{\omega_0 t}{2}\right) \cos(k_1 \omega_0 t) + \sin(k_2 \omega_0 t) - \cot\left(\frac{\omega_0 t}{2}\right) \cos(k_2 \omega_0 t) \right] \\
& - I_1 \left[ 1 - e^{-A(\omega_0 t)^2} \right] \csc\left(\frac{\omega_0 t}{2}\right) \sin\left[\frac{1}{2}(1-k_1+k_2)\omega_0 t\right] \sin\left[\frac{1}{2}(k_1+k_2)\omega_0 t\right] \quad (44)
\end{aligned}$$

Equation (44) gives the total current as a function of time for a set of adjacent harmonics in any interval for which  $k_1 \leq k \leq k_2$  with an ideal mode-locked laser that is started at time  $t$  equal to zero and continues with infinite coherence length to infinity. Note that the second term differs in that decays to zero leaving only the first term which repeats the interval for  $\omega_0 t$  from 0 to  $2\pi$ .

However, for an actual mode-locked laser which has a finite coherence length the process for generating the harmonics restarts at the end of each burst of pulses from the laser. Thus, both terms in Eq. (44) must be used repeatedly to model each restart of lasing. In the examples that are

shown in Section 14 it will be seen that the total current with a set of adjacent harmonics is maximum at the start and end of each cycle of the laser. Thus, shortening the coherence length of a mode-locked laser may actually increase the output power at the harmonics by increasing the relative contribution from that near the beginning and the end of each cycle.

### 10. Interference in sets of adjacent harmonics well below cutoff

The current at each harmonic is zero at the exact start and end of each period of the laser. If the laser had an infinite coherence length and operated well below the cutoff, the total current during each period would have maxima and minima at the ends which decay progressively to smaller magnitudes near the center of the period. This is shown in the examples for Section 14. Now, we examine the mechanism for these effects.

Regrouping the terms in Eq. (12) gives Eq. (45). Then, using the trigonometric identities in Eqs. (46) and (47), we obtain Eq. (48). Finally, simplifying Eq. (48) gives Eq. (49).

$$I(t) = \frac{I_1}{2} \left[ \begin{array}{l} \sin(k_1\omega_0 t) + \sin(k_2\omega_0 t) \\ + \cot\left(\frac{\omega_0 t}{2}\right) [\cos(k_1\omega_0 t) - \cos(k_2\omega_0 t)] \end{array} \right] \quad (45)$$

$$\sin(\alpha) + \sin(\beta) \equiv 2 \sin\left[\frac{\alpha + \beta}{2}\right] \cos\left[\frac{\alpha - \beta}{2}\right] \quad (46)$$

$$\cos(\alpha) - \cos(\beta) \equiv -2 \sin\left[\frac{\alpha + \beta}{2}\right] \sin\left[\frac{\alpha - \beta}{2}\right] \quad (47)$$

$$I(t) = \frac{I_1}{2} \left[ \begin{array}{l} 2 \sin\left[\frac{(k_2 + k_1)\omega_0 t}{2}\right] \cos\left[\frac{(k_2 - k_1)\omega_0 t}{2}\right] \\ + 2 \sin\left[\frac{(k_2 + k_1)\omega_0 t}{2}\right] \sin\left[\frac{(k_2 - k_1)\omega_0 t}{2}\right] \cot\left(\frac{\omega_0 t}{2}\right) \end{array} \right] \quad (48)$$

$$I(t) = I_1 \sin\left[\frac{(k_2 + k_1)\omega_0 t}{2}\right] \left[ \begin{array}{l} \cos\left[\frac{(k_2 - k_1)\omega_0 t}{2}\right] \\ + \sin\left[\frac{(k_2 - k_1)\omega_0 t}{2}\right] \cot\left(\frac{\omega_0 t}{2}\right) \end{array} \right] \quad (49)$$

The first term in brackets for Eq. (49) shows that the total current is zero at a sequence of times given by Eq. (50) where  $n$  may be any positive integer less than  $k_1 + k_2$ . Note that these nulls necessarily occur at closer intervals when either  $k_1$  or  $k_2$  is increased. For example, with  $k_1$  equal to 1 and  $k_2$  equal to 5 there would be 5 nulls within each period of the laser, where  $t_n/T$  is  $1/6, 2/6, 3/6, 4/6,$  and  $5/6$ . Also, with  $k_1$  equal to 1 and  $k_2$  equal to 10 there would be 10 nulls. In general, there are  $k_2 - k_1 + 1$  nulls which is the number of harmonics.

$$\frac{t_n}{T} = \frac{n}{(k_1 + k_2)} \quad (50)$$

An analysis in the appendix shows that the zeros given by setting the second term in the brackets to zero coincide with those just determined in Eq. (50) for the base where the first term is zero.

## 11. Limit for the time-dependent current in a large set of adjacent harmonics

The current in the harmonics is zero at the exact beginning or end of each laser period. However, the current has a dominant positive peak near the beginning and a dominant negative peak near the end with additional positive and negative peaks having lower magnitude in the body of each laser period. Increasing the total number of the harmonics increases the magnitude of the dominant peaks while increasing the rate of the decay of the consecutive extrema when approaching the center of each period. Other phenomena occur near the cutoff that are not considered in this section.

No one has yet measured the time-dependent current at the harmonics, but now we use the identity in Eq. (51) [8] to derive an approximate expression for the current when it is well below the cutoff.

$$\sum_{k=1}^{\infty} \sin(kA) \equiv \frac{\sin(C)}{2[1-\cos(C)]} \text{ for } C > 0 \quad (51)$$

We use Eq. (52) for the current in the frequency domain to include all of the harmonics, but again, we neglect the effects of cutoff that are shown in Eq. (10).

$$I(t) = I_1 \sum_{k=1}^{\infty} \sin(k\omega_0 t) \quad (52)$$

We use Eq. (52) to show that the quantity C in Eq. (51) is  $\omega_0 t$  and then combine Eq. (51) with Eq. (52) to obtain Eq. (53) as an approximation for the total current as a function of time. By inspection, Eq. (53) is singular when  $\omega_0 t$  is an even integer and zero when  $\omega_0 t$  is an odd integer. Thus, the Fourier series in Eq. (52) is singular at these values but this is because we have assumed an infinite series without including the effects of the cutoff.

$$I(t) = \frac{I_1 \sin(\omega_0 t)}{2[1-\cos(\omega_0 t)]} \quad (53)$$

## 12. Derivation of the total RMS current in the harmonics within the nanocircuit

We have made large sets of numerical simulations in which  $k_1$  and  $k_2$  were specified and Eq. (12) was used to obtain sequences of values for the ratio of the normalized time-dependent current, defined as  $I(t)/I_1$ , at evenly-spaced times covering the full range from  $0 < \omega_0 t < 2\pi$ . This is one full period at the laser pulse repetition rate  $\omega_0$  so these currents would be repeated ad-infinitum with an ideal laser.

To clarify the notation, in Eq. (54) we define the symbol “K” to represent the total number of adjacent harmonics. The sum of the squares for the ratio  $I(t)/I_1$  at each specified time was calculated and divided by the number of samples to determine the mean value. Thus, the RHS of Eq. (55) is one-half of the number of harmonics and Eq. (56) gives the normalized RMS value of the total current in the full set of the harmonics from  $k_1$  to  $k_2$ .

$$K \equiv k_2 - k_1 + 1 \quad (54)$$

$$\left( \frac{I_{k_1, n_2}}{I_1} \right)^2 = \frac{K}{2} \quad (55)$$

$$\frac{I_{k_1, k_2, RMS}}{I_1} = \sqrt{\frac{K}{2}} \quad (56)$$

Equation (55) shows that the total power delivered to a load with resistance  $R_L$  is given by Eq. (57) which is exactly the product of the total number of harmonics in this set multiplied by the power that would be delivered at the first harmonic because  $I_1$  is the peak value of the current at that harmonic. However, the transmitting antenna in the nanocircuit has a frequency-dependent impedance consisting of its loss-resistance, radiation-resistance, and reactance so Eq. (57) does not give the full answer for the radiated power. In Section 13 we consider one possibility for this antenna.

$$P_R = K \frac{I_1^2 R_L}{2} \quad (57)$$

### 13. Transmitting antennas for the nanocircuit

We will list several types of the transmitting antennas that may be used in different applications for these nanocircuits. First, we consider the dipole antenna shown in Fig. 2. The radiation resistance  $R_R$  of a thin-wire dipole antenna with length  $L$  is given by Eq. (58) [9] which we have verified. Here  $\eta \approx 376.73 \Omega$  is the impedance of free-space,  $\gamma \approx 0.57722$  is Euler's constant,  $\lambda$  is the wavelength, and  $Ci(x)$  and  $Si(x)$  are the cosine and sine integral functions. The load resistance  $R_L$  of the antenna, which depends on the resistivity and the dimensions of the dipole has been plotted with the radiation resistance,  $R_R$ , in the reference by Balanis [9].

$$R_R = \frac{\eta}{2\pi} \left\{ \begin{array}{l} \gamma + \ln\left(\frac{2\pi L}{\lambda}\right) - Ci\left(\frac{2\pi L}{\lambda}\right) + \frac{1}{2} \sin\left(\frac{2\pi L}{\lambda}\right) \left[ Si\left(\frac{4\pi L}{\lambda}\right) - 2Si\left(\frac{2\pi L}{\lambda}\right) \right] \\ + \frac{1}{2} \cos\left(\frac{2\pi L}{\lambda}\right) \left[ \gamma + \ln\left(\frac{\pi L}{\lambda}\right) + Ci\left(\frac{4\pi L}{\lambda}\right) - 2Ci\left(\frac{2\pi L}{\lambda}\right) \right] \end{array} \right\} \quad (58)$$

Equation (58) shows that the radiation resistance and the load resistance are both maximum when the dipole-length is an even-multiple of half a wavelength, and minimum when the dipole-length is an odd-multiple of half a wavelength. However, the ratio of the load resistance to the radiation resistance at their common maxima becomes large at even number of half-wavelengths and near unity at odd multiples of one half-wavelength. Thus, the transmitted power, which is proportional to the ratio of the ratio of  $R_R$  to  $R_L$ , is maximum when the dipole-length is an odd multiple of one-half-wavelength and minimum for even multiples of one-half wavelength. This relationship may be used to divide the harmonics into groups. Others have used long-wire antennas consisting of a gold thin-film line making an ohmic contact on a semiconductor substrate to detect  $CO_2$  laser radiation [10]. Because they only used the laser frequency, they did not see the broad-band features that are possible with this type of antenna.

These principles may be applied to make much larger devices but, even at the cutoff frequency of 45 THz each monopole in the half-wavelength dipole must have a length of  $1.7 \mu\text{m}$  which would not permit a nanoscale device. Thus, we consider the possibility of having dipoles with a much smaller length. Using asymptotic expansions of the  $Ci$  and  $Si$  functions in Eq. (58) gives Eq. (59) which is generally used by others [11] as the radiation resistance of a short dipole antenna.

$$R_r = \frac{\pi\eta}{6} \left(\frac{L}{\lambda}\right)^2 \quad (59)$$

It is important to recognize that the combination of an extremely high-power flux density from the laser and the unusually high signal-to-noise ratio that we have already measured in the

harmonics with an STM may enable the detection of the power that is transmitted by antennas even when these antennas are unusually short with a very small radiation resistance. Furthermore, the components of the nanocircuits will have a size that is considerably less than that of the tip and the sample electrodes in an STM which will increase the ratio of the surface area to the mass to provide much greater heat transfer, thus enabling the use of much higher current densities which will increase the radiated power.

A variety of electrically-small antennas have been described [12] which may be considered for use in place of the linear dipole that we showed in Fig. 2. We are particularly interested in the recent simulations of the “frequency-independent” square Archimedean spiral antenna [13] because it may be simpler to fabricate in the nanocircuits. This is one of many possibilities for increasing the usable bandwidth of an antenna by using a two-dimensional design instead of a linear antenna. Simulations of the square Archimedean spiral antenna [13], as well as the recent simulations and measurements that have been made for the traditional circular Archimedean spiral [14], [15], [16], show that these antennas have unusually large usable bandwidths so it is surprising that the Archimedean spiral antenna was not mentioned in the extensive summary of small antennas by Hansen and Collin [12].

The configuration that is shown in Fig. 5 could be used in the nanocircuits as shown in the sketch for Fig. 6. Our calculations suggest that by using many turns in a small area the radiation resistance for this antenna exceeds that of a linear dipole shown in Fig. 2. The resistor at the center of the antenna in Fig. 5 and Fig. 6 corresponds to the resistor that is shown in Fig. 2, but now this resistor may not be required.

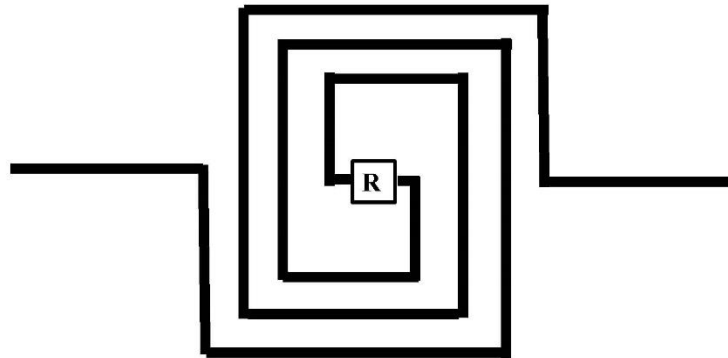


Fig. 5. Archimedean spiral antenna with resistive load at the center.

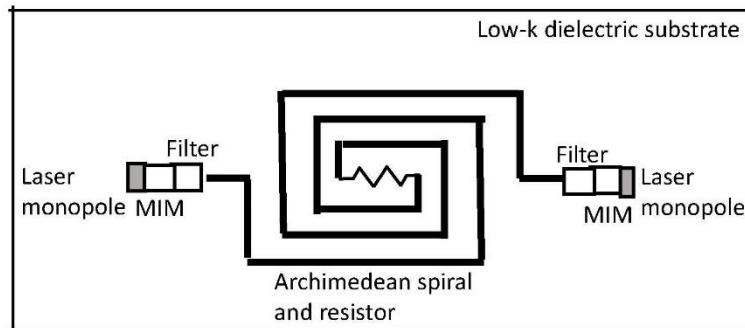


Fig. 6. Sketch of the nanocircuit with an Archimedean spiral antenna

## 14. Examples of simulations

The simulations for examples 1 through 7 were made by using analytical expressions for the tunneling current to follow this current by time-stepping over one or more periods of the mode-locked laser. Example 8 is an analytical solution corresponding to an infinite number of adjacent harmonics. In each of the eight examples the results are presented for one period of the oscillations so the time satisfies  $0 \leq \omega_0 t \leq 2\pi$  radians. A discussion of the phenomena in these eight examples follows at the end of their presentation.

Example 1 (Fig. 7) shows the total normalized current  $I(t)/I_1$  in the 10 adjacent harmonics where  $k_1$  is 1 and  $k_2$  is 10 as calculated using Eq. (12). There are 10 consecutive pairs or minima and maxima in Fig. 7 which correspond to the number of harmonics and this is also seen in Figs. 8 through 11. This is consistent with using Eq. (50) to predict the number of nulls in a given set of adjacent harmonics.

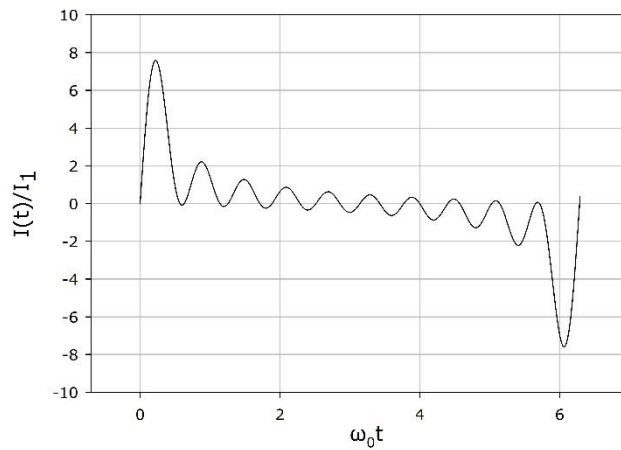


Fig. 7. Normalized total current for 10 adjacent harmonics with indices from 1 through 10.

Example 2 (Fig. 8) shows the total normalized current  $I(t)/I_1$  in the 50 adjacent harmonics where  $k_1$  is 1 and  $k_2$  is 50 as calculated using Eq. (12).

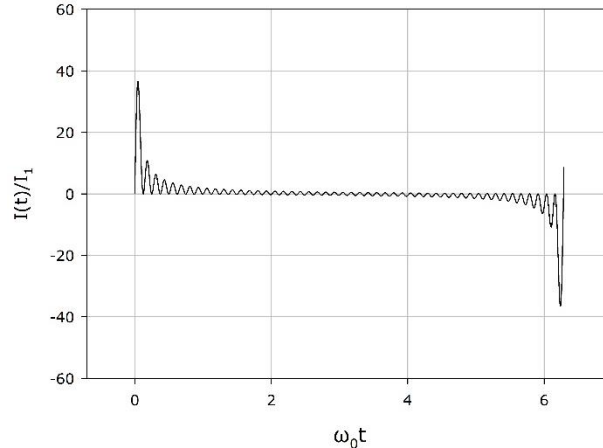


Fig. 8. Normalized total current for 50 adjacent harmonics with indices from 1 through 50.

Example 3 (Fig. 9) shows the total normalized current  $I(t)/I_1$  in the 100 adjacent harmonics where  $k_1$  is 1 and  $k_2$  is 100 as calculated using Eq. (12).

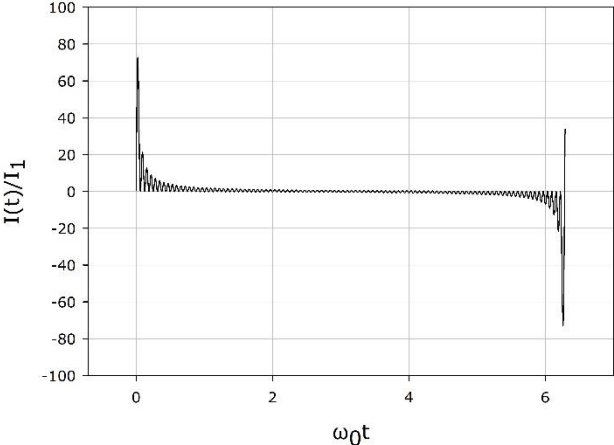


Fig 9. Normalized total current for 100 adjacent harmonics with indices from 1 through 100.

Example 4 (Fig. 10) shows the total normalized current  $I(t)/I_1$  in the 500 adjacent harmonics where  $k_1$  is 1 and  $k_2$  is 500 as calculated using Eq. (12).

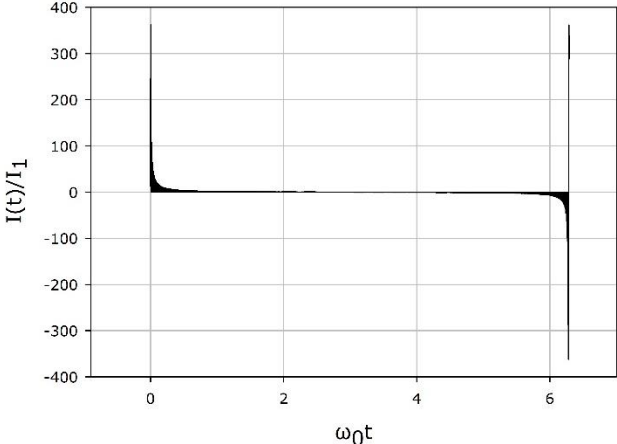


Fig. 10. Normalized total current for 500 adjacent harmonics with indices from 1 through 500.

Example 5 (Fig. 11) shows the total normalized current  $I(t)/I_1$  in the 20 adjacent harmonics where  $k_1$  is 100 and  $k_2$  is 120 as calculated using Eq. (12).

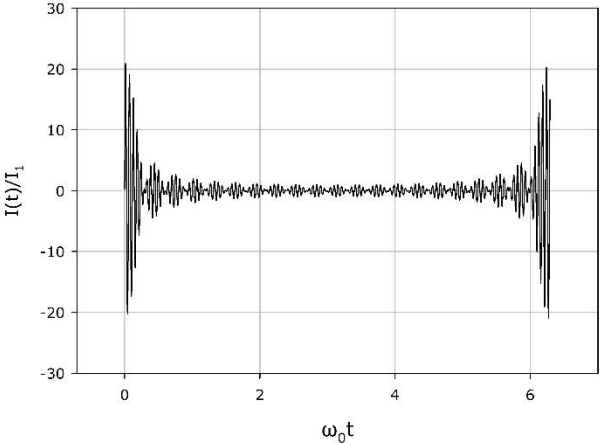


Fig. 11. Normalized total current for 20 adjacent harmonics with indices from 100 through 120.

Example 6 (Fig. 12) shows the total normalized current  $I(t)/I_1$  in the 20 adjacent harmonics where  $k_1$  is 1000 and  $k_2$  is 1020 as calculated using Eq. (12).

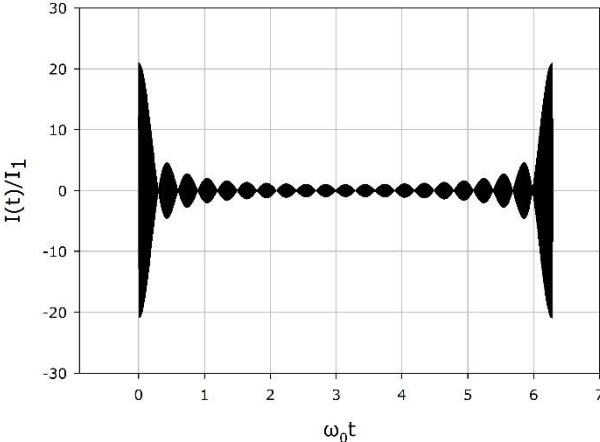


Fig. 12. Normalized total current for 20 adjacent harmonics with indices from 1000 through 1020.

Example 7 (Fig. 13) shows the total normalized current  $I(t)/I_1$  in the 200 adjacent harmonics where  $k_1$  is 1000 and  $k_2$  is 1200 as calculated using Eq. (12).

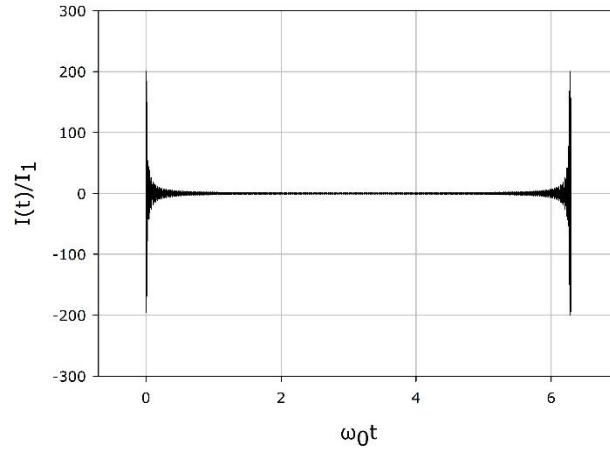


Fig. 13. Normalized total current for 200 adjacent harmonics with indices from 1000 through 1200.

Example 8 (Fig. 14) shows the total normalized current  $I(t)/I_1$  determined using Eq. (56). This corresponds to an infinite number of adjacent harmonics with indices from 1 to infinity. However, the effects of the exponential roll-off of the harmonics at the cutoff are not included in this calculation. Thus, there are singularities in place of the sharp rise and fall at the ends of the period.

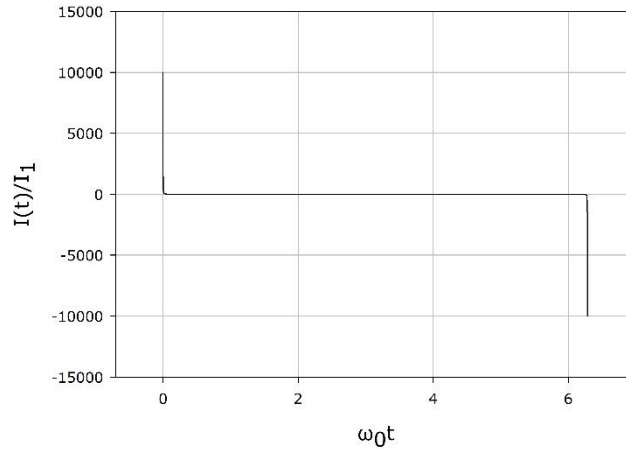


Fig. 14. Normalized total current calculated with Eq. 56 corresponding to an infinite number of adjacent harmonics.

In examples 1 through 4, Figs. 7, 8, 9 and 10, where the adjacent harmonics begin with  $k_1$  equal to 1, the total current has a positive maximum near the beginning and a negative extremum near the end of each period. This may be understood because all of the sinusoids have zero amplitude at both ends and they have different frequencies. Thus, increasing the number of harmonics increases the magnitudes of the extrema at the ends as well as the rate of decay toward the center of each period. In example 8, which approximates having an infinite number of adjacent harmonics, there are singularities at both ends of each period.

In examples 5, 6, and 7, Figs. 11, 12, and 13 each have a group of sinusoidal pulses that are caused by  $k_1$  being different from 1. In example 5, shown in Fig. 11,  $k_1$  is 100 and  $k_2$  is 120 so  $k_2$  minus  $k_1$  is 20 and there are 20 sinusoidal pulses. In example 6, shown in Fig. 12,  $k_1$  is 1000

and  $k_2$  is 1020 so  $k_2$  minus  $k_1$  is 20 and there are again 20 sinusoidal pulses. In example 7, shown in Fig. 13,  $k_1$  is 1000 and  $k_2$  is 1200 so  $k_2$  minus  $k_1$  is 200 and there are 200 sinusoidal pulses but they are difficult to see in this figure because they are small. The result in each of these three examples may be understood by considering the summation from  $k_1$  to  $k_2$  in Eq. (49) as the sum from 1 to  $k_2$  minus the sum from 1 to  $k_1$  as shown in Eq. (60).

$$I(t) = I_1 \sin \left[ (k_2 + 1) \frac{\omega_0 t}{2} \right] \left[ \begin{array}{l} \cos \left[ (k_2 - 1) \frac{\omega_0 t}{2} \right] \\ + \sin \left[ (k_2 - 1) \frac{\omega_0 t}{2} \right] \cot \left( \frac{\omega_0 t}{2} \right) \end{array} \right] - I_1 \sin \left[ (k_1 + 1) \frac{\omega_0 t}{2} \right] \left[ \begin{array}{l} \cos \left[ (k_1 - 1) \frac{\omega_0 t}{2} \right] \\ + \sin \left[ (k_1 - 1) \frac{\omega_0 t}{2} \right] \cot \left( \frac{\omega_0 t}{2} \right) \end{array} \right] \quad (60)$$

In examples 1 through 7 Eq. (12) was used to make independent calculations of the total current at a large number of time-steps on consecutive rows of an Excel file over one full cycle of the laser with corresponding to times from zero to  $2\pi/\omega_0$ . While time-steps of equal size were used in each simulation this is not necessary because each calculation is independent. Furthermore, it would be possible to repeat the calculations at each time-step with different pairs of values for  $k_1$  and  $k_2$  and then add the results at each time-step to determine the total current for the superposition of several groups of adjacent harmonics. It should be clear that all harmonics are inherently present but specifying values of  $k_1$  and  $k_2$  is necessary to determine which are passed by the filters as well as the effects of the transmitting antenna.

Table 1 gives the values of  $\omega_0 t$  and the normalized current  $I/I_1$  that correspond to the first peak in the current for sets of adjacent harmonics calculated using Eq. (49) with specified values of the parameters  $k_1$  and  $k_2$ . The values in this table show that as the number of harmonics is increased the first peak moves toward the left end of the period and the magnitude of this peak becomes greater as may be seen in the Figs. 7 through 13.

Table 1. First peak in the total current with sets of adjacent harmonics.

$k_1$	$k_2$	$\omega_0 t$	Max $I/I_1$
1	2	0.93593	1.7602
1	3	0.66729	2.4996
1	4	0.51861	3.2324
1	5	0.42416	3.9622
1	6	0.35883	4.6904
1	7	0.310943	5.4176
1	8	0.27434	6.1442
1	9	0.24544	6.8704
1	10	0.22206	7.5963
1	11	0.20274	8.3220
1	12	0.18652	9.0475

The creation of intense currents having opposite polarities in the sudden transitions at the start and finish of each laser pulse, is expected to result in partial cancellation of the harmonics which may reduce the output power in the limit as many harmonics are used. This effect may be mitigated in practice by following one or more of the following three procedures: The first method is to reduce the coherence length of the laser as described at the end of Section 9. The second method is to use a moderate number of harmonics chosen for maximum power with stable operation. The third method is to use multiple non-overlapping sets of harmonics. We anticipate that shortening the coherence length of the laser would also increase the power at the harmonics in our measurements with a scanning tunneling microscope but we have not had the opportunity to test this hypothesis. For example, this method could be applied by using harmonics near the different maxima of the radiation resistance for a long-wire antenna that were described in Section 13.

### **15. Suggestions for optimizing the nanocircuits in microwave and terahertz applications**

It is possible to transmit one or more harmonics and the radiated power is increased by raising this number. At microwave frequencies filters can permit the transmission of only a single harmonic or several chosen harmonics. However, groups of adjacent harmonics must be used at terahertz frequencies because of fundamental limitations in the sharpness of the cutoffs for filters. The long-wire antennas described in Section 13 may be used to transmit groups of 1 or more microwave harmonics at frequencies where Eq. (58) shows that the length of the dipole is near an even multiple of one-half of the wavelength. Long-wire antennas could also be used to transmit one or more selected groups of terahertz harmonics at frequencies where the dipole-length is near an even multiple of one-half of the wavelength.

It is possible to use different types of sensors as parts in the two filters of the nanocircuit. These filters could also modulate the harmonics in order to transmit data such as local values for the temperature, ionizing radiation, presence of specific chemicals, or other phenomena, so that one, or even many, nanocircuits could provide such data at high-speed with extremely fine spatial resolution.

### **16. Summary and Conclusions**

We derived a number of new equations to study the harmonics that include the following: Eq. 10 in Section 6 is the general expression for the current in any set of the harmonics.

Eq. 12 in Section 7 is a closed-form expression for the current in a set of adjacent harmonics well below the cutoff.

Eq. 23 in Section 8 is a closed-form expression for the current in a set of adjacent harmonics near the cutoff.

Eq. 44 in Section 9 is a closed-form expression for the current in any set of adjacent harmonics.

Eq. 53 in Section 11 is a closed-form expression for the current in any large set of adjacent harmonics but neglects the exponential at the cutoff.

Eq. 57 in Section 12 is a closed-form expression that may be used to determine the total power in any set of adjacent harmonics neglecting the effects of the cutoff.

Section 1 summarizes our previous related measurements using a mode-locked laser with an STM at microwave frequencies.

Sections 2 and 3 describe the proposed nanocircuit for making measurements at much higher frequencies.

Section 13 describes transmitting antennas for the nanocircuit.

Section 10 describes the phenomena that cause interference of the harmonics, and the examples in Section 14 illustrate these phenomena. Suggestions for optimizing the performance of nanocircuits in microwave and terahertz applications are given in Section 15.

### **Acknowledgments**

We are grateful to the Center for Integrated Nanotechnologies (CINT) at Los Alamos National Laboratory (LANL) for making it possible for Dr. Hagmann to study laser-assisted tunneling in laser-assisted scanning tunneling microscopy for semi-annual two-week visits from 2008 to 2017. This enabled experimental verification and characterization of the microwave frequency comb generated using a mode-locked laser with a scanning tunneling microscope.

We also acknowledge support from NSF STTR 164881, NSF STTR IIP-0712564, NSF SBIR DMI-0338928, and DOE STTR DE-SC000639 that enabled Dr. Hagmann to develop this technology at NewPath Research L.L.C. Now this will be followed by further research and development in his recent appointment as a Research Professor in Electrical and Computer Engineering at the University of Utah.

We are grateful to Isaac Martin, a contractor to NewPath Research L.L.C., who verified and clarified the interpretation of Eq. (58) presented earlier by Balanis [9], and also prepared the graphs.

### **Data availability statement**

The author has chosen to make data that support the findings of this study available upon reasonable request.

### **References**

1. M.J. Hagmann, A.J. Taylor and D.A. Yarotski, “Observation of 200<sup>th</sup> harmonic with fractional linewidth of  $10^{-10}$  in a microwave frequency comb generated in a tunneling Junction”, *Appl. Phys. Lett.* 101 (2012) 241102.
2. M.J. Hagmann, F.S. Stenger and D.A. Yarotski, “Linewidth of the harmonics in a microwave frequency comb generated by focusing a mode-locked ultrafast laser on a tunneling junction”, *J. Appl. Phys.* 114 (2013) 223107.
3. M.J. Hagmann, D.G. Coombs and D.A. Yarotski, “Periodically pulsed laser-assisted tunneling may generate terahertz radiation”, *J. Vac. Sci. Technol. B* 35 (2017) 03D109.
4. M.J. Hagmann, A. Efimov, A.J. Taylor, and D.A. Yarotski, “Microwave frequency-comb generation in a tunneling junction by intermode mixing of ultrafast laser pulses”, *Appl. Phys. Lett.* 99, 011112 (2011).
5. M.J. Hagmann, P. Andrei, S. Pandey and A. Nahata, “Possible applications of scanning frequency comb microscopy for carrier profiling in semiconductors”, *J. Vac. Sci. Technol. B*, 33 (2015) 02B109 (6 pp).
6. M.J. Hagmann, M.S. Mousa and D.A. Yarotski, “Resolution in carrier profiling semiconductors by scanning spreading resistance microscopy and scanning frequency comb microscopy”, *Appl. Microsc.* 47 (2017) 95-100.
7. M.J. Hagmann, “Scanning frequency comb microscopy—A new method in scanning probe microscopy”, *AIP Advances*, 8 (2018) 125203.
8. A.D. Whealon, *A Short Table of Summable Series*, Report SM-14642, (Space Technology Laboratories, Los Angeles, CA) 1953, p. 58
9. C.A. Balanis, *Antenna Theory* (New York, Wiley) 2nd ed., 1997, pp. 156-157, 488-498.

10. T. Shimizu, Y. Yasuoka, K. Gamo and S. Namba, “Thin-film long-wire antenna for 10.6  $\mu\text{m}$  CO<sub>2</sub> laser radiation”, Jpn. J. Appl. Phys. 31 (1992) 3359-3361.
11. J.D. Kraus, Antennas (New York, McGraw-Hill) 2<sup>nd</sup> ed., 1998, p. 216.
12. R.C. Hansen and R.E. Collin, Small Antenna Handbook (New York, Wiley-IEEE Press, 2012).
13. W. Bousbaa, H. Medkour, F. Bouttout and Z. Messali, “Fully planar frequency independent square Archimedean spiral antenna with impedance transformer for ground penetrating radars”, Micro. Opt. Technol Lett. 63 (2021) 295-309.
14. C. Shemlya, M. Zemba, M. Liang, X. Yu, D. Espalin, R. Wicker, H. Xinand E. MacDonald, “Multi-layer Archimedean spiral antenna fabricated using polymer extrusion 3D printing”, Microw. Opt. Technol. Lett. 58 (2016) 1662-1666.
15. A. Alex-Amor, P. Padilla, J.M. Fernandez-Gonzalez and M. Sierra-Castaner, “A miniaturized ultrawideband Archimedean spiral antenna for low-power sensor applications in energy harvesting”, Microw. Opt. Technol. Lett. 61 (2019) 211-216.
16. E. Akkaya and F. Gunnes, “Ultrawideband, high performance, cavity-backed Archimedean spiral antenna with Phelan balun for direction finding and radar warning receiver applications”, J. RF Microw. Comput. Aided Eng. 31 (2021) 1-18.

### Appendix: Second possibility for zeros in the total current

In Section 10 we derived Eq. (49) for the total current in a set of adjacent harmonics with indices from  $k_1$  to  $k_2$  and Eq. (50) for the set of times at which the first of the two terms within brackets in Eq. (49) is zero. Now we determine if there are other values of  $\omega_0 t$  for which the second term, which is shown as Eq. (A1), is zero.

$$\text{Term2} \equiv \cos\left[\left(k_2 - k_1\right)\frac{\omega_0 t}{2}\right] + \sin\left[\left(k_2 - k_1\right)\frac{\omega_0 t}{2}\right] \cot\left(\frac{\omega_0 t}{2}\right) \quad (\text{A1})$$

The definition of  $K$  in Eq. (50) is used with Eq. (A1) to give Eq. (A2).

$$\text{Term2} = \cos\left[\left(K - 1\right)\frac{\omega_0 t}{2}\right] + \sin\left[\left(K - 1\right)\frac{\omega_0 t}{2}\right] \cot\left(\frac{\omega_0 t}{2}\right) \quad (\text{A2})$$

At the start and end of each cycle of the laser, where  $\omega_0 t$  is an integral multiple of  $2\pi$ , the second part of Eq. (A2) is zero because the sine function is zero. However, the first term is plus or minus 1. Therefore, the points at the beginning and end of each cycle are excluded from the search for possible roots from the second term. Thus, we divide by the sine term in Eq. (A2) to obtain Eq. (A3) as the condition for which the second term of Eq. (49) could possibly be zero.

$$\cot\left[\left(K - 1\right)\frac{\omega_0 t}{2}\right] = -\cot\left(\frac{\omega_0 t}{2}\right) \quad (\text{A3})$$

When  $x$ , as defined in Eq. (A4), is substituted into Eq. (A3) this gives Eq. (A5) where  $N$  must be an integer of 1 or greater so we search for values of  $x$  that satisfy Eq. (A5) over the interval  $0 \leq \omega_0 t \leq 2\pi$  which corresponds to one period of the cotangent function from  $0 \leq x \leq \pi$ .

$$x \equiv \frac{\omega_0 t}{2} \quad (\text{A4})$$

$$\cot\left[\left(K - 1\right)x\right] + \cot(x) = 0 \quad (\text{A5})$$

The following solutions, derived using Wolfram Alpha and then verified numerically by substitution using bisection for high-accuracy. They correspond to the set of values for  $x$  between 0 and  $\pi$  that satisfy Eq. (A5) for each value of  $K$ . When  $K = 1$ ,  $x_1 = \pi/3$  and  $x_2 = 2\pi/3$ . When  $K =$

2,  $x_1 = \pi/4$ ,  $x_2 = 2\pi/4$ , and  $x_3 = 3\pi/4$ . When  $K = 3$ ,  $x_1 = 2\pi/10$ ,  $x_2 = 4\pi/10$ ,  $x_3 = 6\pi/10$ , and  $x_4 = 8\pi/10$ . Table A1 shows the corresponding normalized times,  $t/T$  as fractions, in one period of the mode-locked laser, at which the total current of the harmonics is zero.

Table A1. Normalized times for zero total current in one the period for the laser with Eq. A-5.

K	Normalized times for zero current in one period of the laser, $t/T$					
1	1/3		2/3			
2	1/4	2/4		3/4		
3	1/5	2/5	3/5		4/5	
4	1/6	2/6	3/6	4/6	5/6	
5	1/7	2/7	3/7	4/7	5/7	6/7

The values in Table A1, which were determined by setting the second bracketed term in Eq. (49) to zero, are identical to those we derived earlier in Section 9 by setting the first bracketed term in Eq. (49) to zero. Thus, this appendix shows that no additional zeros are caused by the second term.